The Duffing Oscillator

Alexei Stepanenko u6124616

April 19, 2017

Contents

1 Introduction

In this report, we provide an analysis of a wide variety of aspects of the Duffing oscillator, using both numerical and analytical techniques. The Duffing oscillator is an interesting system to study beaus of the complexity of the dynamical behavior it exhibits, despite its simplicity.

1.1 Equations Of Motion

The Duffing oscillator is a one dimensional damped driven oscillator in a double well potential. It is described by the second order differential equation

$$\ddot{x} + 2\gamma\dot{x} + \alpha x + \beta x^3 = F\cos(\omega t). \tag{1}$$

The Lagrangian that generates these equations of motion includes a factor $e^{2\gamma t}$ due to the dissipation term $2\gamma\dot{x}$. The Lagrangian for the Duffing oscillator is

$$L = e^{2\gamma t}(\frac{1}{2}\dot{x}^2 - \frac{1}{2}\alpha x^2 - \frac{1}{4}\beta x^4 - Fx\cos(\omega t)). \tag{2}$$

Then the Euler-Lagrange equations generate the equations of motion,

$$\begin{aligned} \frac{d}{dt}(\frac{\partial L}{\partial \dot{x}}) - \frac{\partial L}{\partial x} &= 0 \\ \Rightarrow (\ddot{x} + 2\gamma\dot{x} + \alpha x + \beta x^3 - F\cos(\omega t))e^{2\gamma t} &= 0 \\ \Rightarrow \ddot{x} + 2\gamma\dot{x} + \alpha x + \beta x^3 &= F\cos(\omega t). \end{aligned}$$

1.2 Parameters

The Duffing oscillator in the form (1) has 5 real physical parameters: γ, α, β, F and ω. We work in SI units throughout with m and s denoting meters and seconds respectively,

- γ is assumed to the greater than or equal to zero. It describes the magnitude of damping that the system undergoes and it has units s^{-1}.
- F describes the magnitude of the driving force. F has units ms^{-2}. A negative value of F corresponds to a change in phase of magnitude π of the driving force.
- ω describes the frequency of the driving force. ω has units s^{-1}. The sign of ωdoes not affect the dynamics of the system because cosine is an even function.
- α and β describe the shape of the double well potential. α and β have units s^{-2} and $m^{-2}s^{-2}$ respectively. Referring to the Lagrangian (2), the double well potential is given by

  $$V = \frac{1}{2}\alpha x^2 + \frac{1}{4}\beta x^4.$$

  We impose that $\alpha < 0$ and $\beta > 0$. Firstly, this ensures that the potential has a local maximum stationary point at $x = 0$. This restriction also implies that $V \to \infty$ as $x \to \pm\infty$, ensuring that the trajectories of the system are bounded. The potential V has minima at $x = \pm\sqrt{\frac{-\alpha}{\beta}}$ and the difference in potential between the local maximum stationary point and the minima (in other words, the size of the central hump) is $\frac{3}{4}\frac{\alpha^2}{\beta}$. Hence the ratio between α and β indicates the 'size' of the double-well potential.

1.3 Dimensionless Form

We will now derive the dimensionless form of the equations of motion (1). One reason for doing this is that the parameters will become dimensionless. Dimensionless parameters are combinations of the physical parameter that affect the dynamics in a more direct way to the physical parameters and hence can be considered more important. For example, consider increase the magnitude of the driving force F while also increasing the size of the potential by increasing α and decreasing β and appropriate amount. Then we can expect similar qualitative dynamics only with x and $\dot{x}$ being scaled by some constant. The dimensionless form of the equations will reduce the number of parameters we have to consider, making them easier to analyse.

There is more than one dimensionless form of (1). We chose a form such that the dimensionless parameters are easy to physically interpret. We define the dimensionless dynamical variable by $q = \frac{x}{x_0}$ where $x_0 = \sqrt{\frac{-\alpha}{\beta}}$ and define $\tau = \frac{t}{t_0}$ where $t_0 = \frac{1}{\sqrt{-\alpha}}$. Next we calculate each term in (1) in terms of q and τ. Firstly,

$$\ddot{x} = \frac{d^2x}{dt^2} = x_0(\frac{d\tau}{dt})^2\frac{d^2q}{d\tau^2} = \frac{x_0}{t_0^2}\ddot{q},$$
$$2\gamma\dot{x} = 2\gamma x_0(\frac{d\tau}{dt})\frac{dq}{d\tau} = 2\gamma\frac{x_0}{t_0}\dot{q}$$

where $\dot{q} \equiv \frac{dq}{d\tau}$ and $\ddot{q} \equiv \frac{d^2q}{d\tau^2}$. We also have that $\alpha x = \alpha x_0 q$, $\beta x^3 = \beta x_0^3 q^3$ and $\omega t = \omega t_0 \tau$, so that (1) becomes,

$$\frac{x_0}{t_0^2}\ddot{q} + 2\gamma\frac{x_0}{t_0}\dot{q} + \alpha x_0 q + \beta x_0^3 q^3 = F\cos(\omega t_0\tau)$$
$$\Rightarrow \ddot{q} + 2\gamma t_0\dot{q} + \alpha t_0^2 q + \beta x_0^2 t_0^2 q^3 = F\frac{t_0^2}{x_0}\cos(\omega t_0\tau).$$

The constants in front of q and q^3 become -1 and 1 respectively leaving us with the dimensionless form of the equations of motion,

$$\ddot{q} + 2b\dot{q} - q + q^3 = A\cos(\Omega\tau), \tag{3}$$

where the new constants are $b = \frac{\gamma}{\sqrt{-\alpha}}$, $A = F\sqrt{\frac{\beta}{-\alpha^3}}$ and $\Omega = \frac{\omega}{\sqrt{-\alpha}}$. Notice that $b \sim \gamma$, $A \sim F$ and $\Omega \sim \omega$, so that we can physically interpret b, A, & Ω as re-scaled damping, driving force and driving frequency respectively.

1.4 Autonomous Form

The equations of motion for the Duffing oscillator are non-autonomous, meaning that they explicitly depend on time. It is possible to make the equations formally non-autonomous in the following way. Let $p = \dot{q}$ and $z = \Omega t \mod 2\pi$. Then (3) becomes

$$\frac{d}{d\tau}\begin{bmatrix} q \\ p \\ z \end{bmatrix} = \begin{bmatrix} p \\ -2bp + q - q^3 + A\cos(\Omega z) \\ 1 \end{bmatrix}. \tag{4}$$

Letting

$$\mathbf{r} = \begin{bmatrix} q \\ p \\ z \end{bmatrix}$$

and

$$\mathbf{f} = \begin{bmatrix} p \\ -2bp + q - q^3 + A\cos(z) \\ \Omega \end{bmatrix}$$

the equations of motion can be written simply as

$$\dot{\mathbf{r}} = \mathbf{f}(\mathbf{r}). \tag{5}$$

This provides a more geometric picture of the system. The state space $\mathcal{M}$ can be considered a surface $\mathbb{R}^4$. Formally,

$$\mathcal{M} \cong \mathbb{R}^2 \times S^1,$$

where $S^1 \cong \{w \in \mathbb{R}^2 : |w| = 1\}$ is a circle in $\mathbb{R}^2$. The $\mathbf{f}(\mathbf{r})$ defines a vector field on $\mathcal{M}$ and the trajectories for the system are curves following the vector field (formally known as integral curves of the vector field). We will take advantage of the form (4) of the equations when we study the symmetry of the Duffing oscillator as well as in the next section. The form (4) is also sometimes useful for numerical integration, when we wish to start the trajectory at different phases of the driving force.

2 Phase Plane Analysis

In general, there are no analytical solutions for the Duffing oscillator, so we must find other methods of understanding the system. One method is to numerically integrate the equations of motion. The disadvantage of this is that parameters have to be fixed for numerical integration. In the case that $A = 0$, the state space becomes two dimensional and we can perform a phase plane analysis. Phase plane analysis uses local stability analysis and the smoothness of the flow of the system to obtain a very good understanding of the global qualitative behavior of the system. Because the system is two-dimensional when $A = 0$, Poincareé-Bendixon theorem applies and any trajectory must either tend to a fixed point or tend to a periodic orbit (or be on a fixed point/periodic orbit).

2.1 Fixed Points

An fixed point is a point in the state space that does not change as time evolves. If $\mathbf{r}_*$is an fixed point then $\dot{\mathbf{r}}_* = 0$, hence, $\mathbf{f}(\mathbf{r}_*) = 0$. When $A > 0$, $\mathbf{f}(\mathbf{r}) = 0$ has no solutions because the variable we introduce to make the system autonomous is constantly equal to one, so there do not exist any fixed points when $A \neq 0$. When $A = 0$, the equations of motion (4) become

$$\dot{\mathbf{u}} = \mathbf{v}(\mathbf{u}), \tag{6}$$

where

$$\mathbf{u} = \begin{bmatrix} q \\ p \end{bmatrix}$$

and

$$\mathbf{v} = \begin{bmatrix} p \\ -2bp + q - q^3 \end{bmatrix}. \tag{7}$$

The condition that $\mathbf{u}_* = (q_*, p_*)$ is a fixed point is

$$\begin{bmatrix} p_* \\ -2bp_* + q_* - q_*^3 \end{bmatrix} = \mathbf{0}.$$

This is implies that any equilibrium point must be stationary, $p_* = 0$, and that

$$\begin{aligned} q_*(1 - q_*^2) &= 0 \\ \Rightarrow q_* &= 0, \pm 1. \end{aligned}$$

So that we have three equilibrium points: $\mathbf{u}_0 = (0, 0)$, $\mathbf{u}_+ = (1, 0)$ and $\mathbf{u}_- = (-1, 0)$.

$\mathbf{u}_0$ corresponds to the state sitting at the local maximum (the center hump) and $\mathbf{u}_\pm$ corresponds to the state sitting at one of the minima (at the bottom of the wells) of the double well potential. Intuitively, it is clear that if we perturb $\mathbf{u}_0$ slightly, the state will fall away the local maximum towards one of the minima, whereas if we perturb $\mathbf{u}_\pm$ slightly the state will fall back towards the fixed point. An asymptotically stable fixed point is one for which there exists a neighborhood in which all the trajectories will remain trapped for all time. An unstable fixed point is one which is not asymptotically stable.

To show this mathematically, consider an fixed point $\mathbf{u}_*$. If the state is in a small neighborhood of $\mathbf{u}_*$ we can approximate the equations of motion (6) by performing a Taylor expansion about $\mathbf{u}_*$ and taking the leading linear term,

$$\begin{aligned} \dot{\mathbf{u}} &\approx \mathbf{v}(\mathbf{u}_*) + Dv|_{u=u_*}(\mathbf{u} - \mathbf{u}_*) \\ \Rightarrow \dot{\mathbf{u}} &\approx Dv|_{u=u_*}(\mathbf{u} - \mathbf{u}_*), \end{aligned} \tag{8}$$

where

$$Dv|_{u=u_*} = \begin{bmatrix} 0 & 1 \\ 1 - 3q_*^2 & -2b \end{bmatrix}$$

is the Jacobian evaluated at the equilibrium point. We can use (7) to obtain qualitative pictures of the flow of trajectories about the fixed point. If $\mathbf{u}$ lies on an eigenvector (that corresponds to a real eigenvalue) of the Jacobian $Dv|_{u=u_*}$, then the acceleration will be along the eigenvector itself so that the state will move along the eigenvector. If the eigenvalue corresponding to that eigenvector is positive, then the state will flow away from the fixed point; if it is positive it will flow towards the fixed point. The continuity of the flow then allows us to draw a *phase portrait* around the fixed point, a qualitative picture of the flow of trajectories around the fixed point. Determining the phase portrait around the fixed will not only allow us to determine the stability of the fixed points, but we can later combine them to obtain a phase portrait for the entire system, giving us an understanding of the flow for the entire phase space.

2.2 Stability Of Fixed Points

2.2.1 Middle Fixed Point: $\mathbf{u_0}$

We start with the middle fixed point $\mathbf{u}_0 = (0, 0)$. The Jacobian evaluated at $\mathbf{u}_0$is

$$Dv|_{u=u_0} = \begin{bmatrix} 0 & 1 \\ 1 & -2b \end{bmatrix}.$$

Let T denote the trace of the Jacobian and let Δ denote the determinant. In this case , $T = -2b$ and $\Delta = -1$. The eigenvalues of the Jacobian are,

$$\begin{aligned}\lambda_{1,2} &= \frac{1}{2}(T \pm \sqrt{T^2 - 4\Delta}) \\ &= \frac{1}{2}(-2b \pm \sqrt{4b^2 + 4}) \\ &= \pm\sqrt{b^2 + 1} - b.\end{aligned}$$

The parameter b which describes the damping strength is assumed to be greater than or equal to zero, so, in all parameter regimes one eigenvalue is positive and one eigenvalue is negative. A fixed point with one positive eigenvalue and one negative eigenvalue is called a *saddle point*. In the linear neighborhood of $\mathbf{u}_0$, a trajectory flows in towards the fixed point along the eigenvector corresponding to the negative eigenvalue (called the *stable eigenvector*) and a trajectory flows out away from the fixed along the eigenvector corresponding to the positive eigenvalue (called the *unstable eigenvector*). Recall that trajectories of the system are really curves following a vector field on the state space defined by (7) in this case. The equations of motion are smooth (i.e. infinitely differentiable) so the vector field is also smooth. This implies that for a small enough neighborhood in the state space all the points in almost the same direction and as we reduce the size the size of this neighborhood to zero the difference in the directions of the trajectories tends to zero. For the neighborhood of our fixed point $\mathbf{u}_0$this implies that all the trajectories around the unstable eigenvector flow away from the fixed point and all the trajectories around the stable eigenvector flow towards the fixed point. The only way for the trajectories to be smooth in this case is for a trajectory starting near the stable eigenvector to first flow towards the fixed point then flow out along the unstable eigenvector. The phase portrait of $\mathbf{u}_0$ is shown in figure 1. $\mathbf{u}_0$ is unstable because the only trajectories that stay close to the fixed point for all time lie on the stable eigenvector.

2.2.2 Outer Fixed Points: $\mathbf{u}_\pm$

Now lets focus on the outer fixed points, $\mathbf{u}_\pm = (\pm 1, 0)$, that have zero velocity and sit in potions corresponding to the bottom of the wells. The Jacobian for these fixed points is

$$Dv|_{u=u_\pm} = \begin{bmatrix} 0 & 1 \\ -2 & -2b \end{bmatrix}.$$

Notice that the Jacobian is identical for $\mathbf{u}_+ = (1, 0)$ and $\mathbf{u}_- = (-1, 0)$, so, the phase portraits around these fixed points will be identical. The trace for the Jacobian is $T = -2b$ and the determinant is $\Delta = 2$. The eigenvalues of the Jacobian are

$$\begin{aligned}\lambda_{1,2} &= \frac{1}{2}(T \pm \sqrt{T^2 - 4\Delta}). \\ &= \frac{1}{2}(-2b \pm \sqrt{4b^2 - 8} \\ &= -b \pm \sqrt{b^2 - 2}.\end{aligned}$$

For the outer fixed points, the phase portrait is different for different values of b. There are three cases which produce qualitatively different behavior in the vicinity of $\mathbf{u}_\pm$: $b = 0$, $0 < b \leqslant \sqrt{2}$ and $b > \sqrt{2}$.

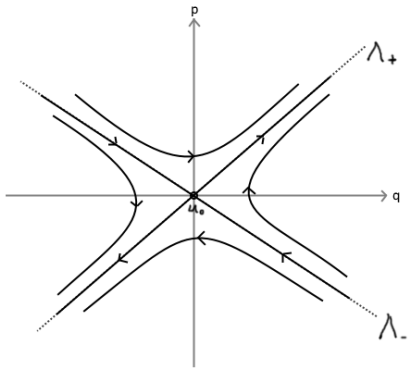

Figure 1: Phase portrait in the neighbourhood of the u_0. Λ_+ denotes the unstable eigenvector and Λ_- denotes the stable eigenvector.

First, lets consider the case where $b > \sqrt{2}$. When $b > \sqrt{2}$, both eigenvalues will be negative. Trajectories along either eigenvector will flow in towards the fixed point. Then by the smoothness of the flow all trajectories will tend towards the fixed point as $t \to \infty$. Any trajectory in the neighborhood where the linear approximation is qualitatively correct will remain in the linear neighborhood for all time so the fixed point is asymptotically stable as expected. One eigenvector will have an eigenvalue that has a larger magnitude than the other. For this eigenvector the flow towards the fixed point will be faster - this causes the trajectories around the eigenvectors to be skewed so that they are more in line with this eigenvector (whose eigenvalue has a larger magnitude) and tend to be parallel with this eigenvector as the trajectories tend to the fixed point. The phase portrait for $\mathbf{u}_\pm$ in the case that $b > \sqrt{2}$ in shown in figure 2 .

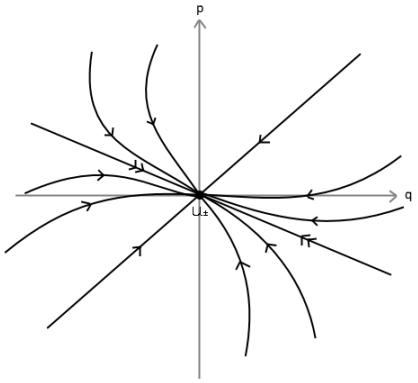

Figure 2: Phase portrait in the neighbourhood of the u_0 in the case that $b > \sqrt{2}$

When $0 < b < \sqrt{2}$, both eigenvalues are complex with a negative real part. In this case, trajectories in the linear neighborhood of $\mathbf{u}_\pm$spiral in towards $\mathbf{u}_\pm$ [5]. This is because the eigenvalues appear inside exponential functions in the solutions to the linearised equations and hence the imaginary parts of the eigenvalues create sinusoidal terms in the solutions while the real negative part causes the solutions to tend towards the fixed point. Since any point in the linear neighborhood will tend towards the fixed point, it is asymptotically stable again in this case. When $b = 0$, the eigenvalues are purely imaginary. With no real in the eigenvalue the trajectories neither tend to the fixed point nor are repelled away from it. In this case, the fixed point is called a *center*. It is considered asymptotically stable because the trajectories are periodic orbits; if a neighborhood contains a periodic orbit that trajectory as well as an infinite number of smaller trajectories will stay in that neighborhood for all time. The phase portraits of $\mathbf{u}_\pm$are shown in figure 3.

2.3 Phase portraits

In this section, we combine the phase portraits for $\mathbf{u}_0$ and $\mathbf{u}_\pm$ to obtain qualitative pictures of the behavior of the system. There are three different cases corresponding to the three cases for $\mathbf{u}_\pm$: $b = 0$, $0 < b \leqslant \sqrt{2}$ and $b > \sqrt{2}$. To combine the phase portraits we must bear in mind that the flow must be smooth and that the trajectories cannot cross (due to this being a deterministic system).. We must also use our intuition to some extent. The phase portraits are shown in figures 4 a)-c). Alongside them are compute generated phase portraits with parameters in the regime that the analytical phase portraits are meant to represent (figure 4 i)-iii). The computer generated phase portraits where made by plotting a number of numerically evaluated trajectories, whose initial conditions form a grid in phase space. The trajectories are all plotted in different colors to help distinguish between them.

When $b = 0$, energy is conserved. There a state on the trajectory that comes from unstable eigenvector of $\mathbf{u}_0$ (called the *unstable manifold*) must eventually come back to the fixed point in the limit $t \to \infty$. It must therefore connect up with the *stable manifold* of $\mathbf{u}_0$, the set of points that tend to $\mathbf{u}_0$ as $t \to \infty$. This trajectory in closed but not periodic is called a *homoclinic orbit*. Trajectories inside this homoclinic orbit must stay inside because trajectories cannot cross. Because $\mathbf{u}_\pm$is a center and lies inside the homoclinic orbit, by the smoothness of the flow, all the trajectories inside the homoclinic orbits must be periodic orbits. Outside the homoclinic orbit, all the trajectories are again periodic orbits due smoothness.

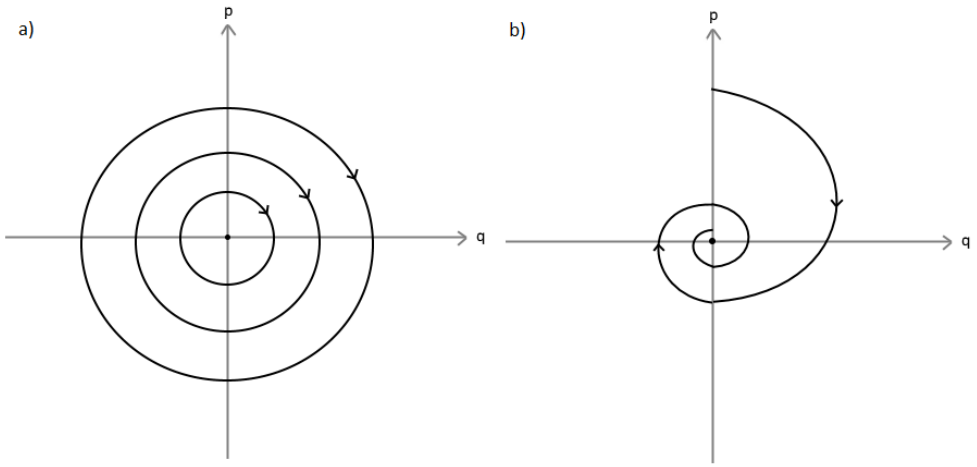

Figure 3: a)Phase portrait in the neighbourhood of $\mathbf{u}_\pm$ for $b = 0$. b) Phase portrait in the neighbourhood of $\mathbf{u}_\pm$ for $0 < b \leqslant \sqrt{2}$

.

When $0 < b \leqslant \sqrt{2}$, the homoclinic orbit breaks apart because a trajectory starting on the will slow down due to the damping and eventually converge to either $\mathbf{u}_+$ or $\mathbf{u}_-$ in a spiral trajectory. The stable manifold of $\mathbf{u}_0$ veers off to infinity as $t \to -\infty$. On the side of the stable manifold contain $\mathbf{u}_+$all the trajectories fall into $\mathbf{u}_+$in a spiral trajectory, circling the fixed points infinity many times. Similarly all the trajectory on the side of the stable manifold contain $\mathbf{u}_-$ fall into $\mathbf{u}_-$ in a spiral pattern.

For $b > \sqrt{2}$, the picture is very similar to the previous case. Again, the stable manifold veers off to infinity as $t \to -\infty$ and partitions the state space into trajectories that fall into $\mathbf{u}_+$ and trajectories that fall into $\mathbf{u}_-$. The main difference in this case is that the trajectories do not circle the fixed point infinity many times as they fall in but align themselves with the stable eigenvector of the Jacobian that has eigenvalue with the larger magnitude.

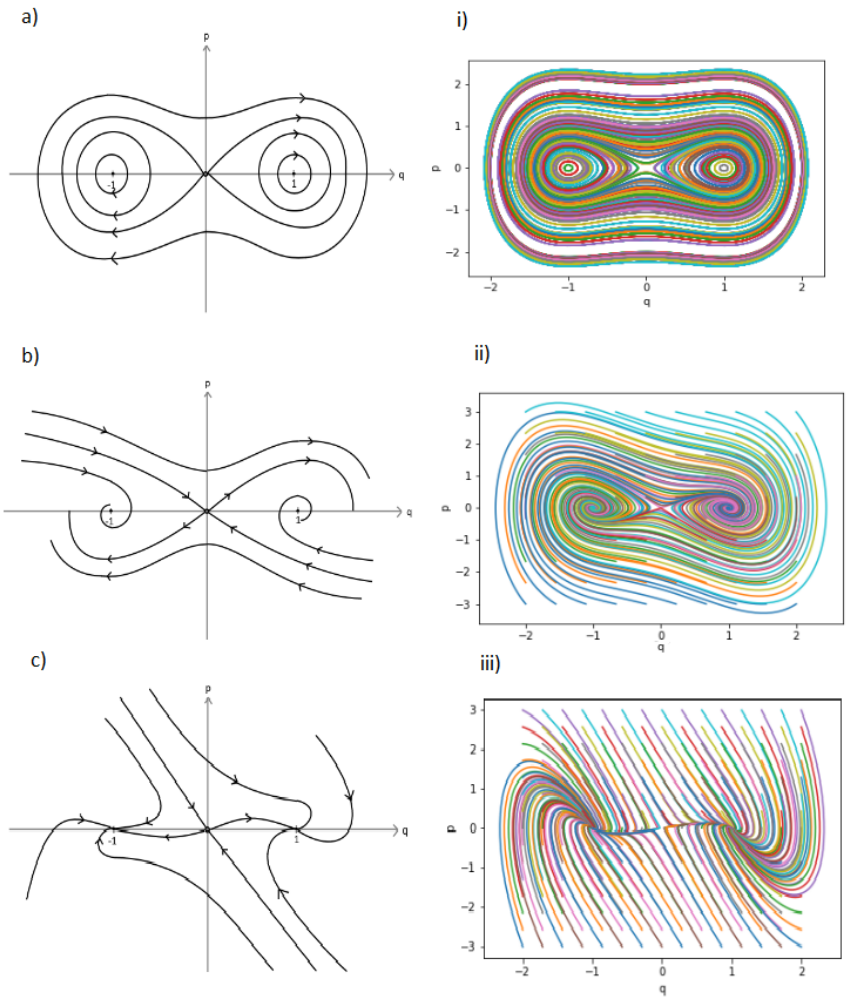

Figure 4: a) Analytical phase portrait for $b = 0$. b) Analytical phase portrait for $0 < b \leqslant \sqrt{2}$. c) Analytical phase portrait for $b > \sqrt{2}$. i) Computer-generated phase portrait for $b = 0$. ii) Computer-generated phase portrait for $b = 0.3$. iii) Computer-generated phase portrait for $b = 1.46$.

3 Numerical Solutions

Now, we begin to investigate the behavior as the system when the driving force is non-zero. Since the phase space is three dimensional in this case, it is possible for the system to exhibit deterministic chaos. However this means that trajectories can intersect in the two dimensional (q, p) phase space, meaning that phase plane analysis is no longer a useful tool. Given specific parameters and initial conditions we can perform numerical integration to find an approximation of the trajectory. We used python to perform the numerical integration, specifically, we used the function odeint in the Python package Scipy. We also built an interactive widget in the Python IDE IPython, in which we could adjust the initial conditions and parameters using sliders, receiving the trajectory plotted in phase space back almost immediately. This streamlined the process of exploration of the behavior of the system in the various parameter regimes. The code is included in the appendix.

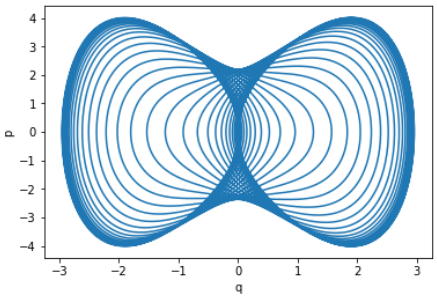

Figure 5: A numerically determined trajectory at parameters $b = 0$, $A = 5$ and $\Omega = 0.03$ with inital conditions $\mathbf{r}(\mathbf{0}) = \mathbf{u_0}$.

Our general approach was to fix two parameters and see how the behavior changed as we varied the other parameter. We fixed $b = 0.15$ and $\Omega = 1$ and varied A. At $A = 0$, all the trajectories spiral into either $\mathbf{u}_+$ or $\mathbf{u}_-$as described in the previous section. When we introduce a small non-zero driving force the system no longer tends to a fixed point but tends to periodic orbit either around $\mathbf{u}_+$or $\mathbf{u}_-$. This sort of periodic orbit to which trajectories asymptotically tend to is called a *limit cycle*. Indeed, this is what we should expect to do. For small enough driving force, the trajectories stay close to either $\mathbf{u}_+$ or $\mathbf{u}_-$. The system will then be approximated very well by a damped driven harmonic oscillator which we know tends to a limit cycle. For example, for the initial condition $\mathbf{r}(0) = \mathbf{u}_-$ with $A = 0.1$, the trajectory expands outwards past the limit cycle, then it falls back inside and tends towards the limit cycle from the inside. For the initial condition $\mathbf{r}(0) = \mathbf{u}_0$, the trajectory tends to a limit cycle around $\mathbf{u}_+$, this is because the driving is initially in the positive direction. As we gradually increase the the driving force A, the qualitative behavior of the system does not initially change. The size of the limit cycles increase as A increase. At around $A = 0.28$, the driving force is strong enough to allow the trajectories to move between the wells. At $A = 0.35$, the trajectories fall into two qualitative classes. For initial conditions where the magnitude of q greater than about 1.5 or the magnitude of p is greater than about 1, the trajectories behave wildly and show no discernible order. For initial conditions where the magnitude of q greater than about 1.5 or the magnitude of p is greater than about 1, the trajectories spiral towards the origin until they the trajectory is inside that region, then the trajectories again behave wildly. This lead us hypothesize that the system exhibits dynamical chaos at parameters $(b, A, \Omega) = (0.15, 0.35, 1)$. The systems continues to behave in a similar way until about $A = 0.55$, when a stable limit cycle again appears, this time passing through both wells.

Some interesting behavior occurs when the $b = 0$. For example, for the parameters $(b, A, \Omega) = (0, 5, 0.03)$ and initial conditions $\mathbf{r}(0) = \mathbf{u}_0$, the trajectory does not seem to follow a periodic orbit (at least not a very short one) but is very ordered. The trajectory is show in figure 5. For high b, the trajectories tend to a limit cycle around $\mathbf{u}_0$ that does not even reach $\mathbf{u}_\pm$; the system is damped so strongly, the driving force reverses before the trajectory manages to reach the bottom of the well.

As mentioned, numerical integration gives only an estimation of a trajectory. Every, integration step produces a small error. Chaotic systems display sensitivity to initial conditions, so this error will amplify.

This makes chaotic systems inherently unpredictable. However, we numerical integration is still a good tool for studying the qualitative behavior of chaotic system. This is because many chaotic systems display shadowing properties [4]; although a numerically evaluated trajectory does diverges from the real trajectory with the same initial condition eventually, there exist a real trajectory that stays close to the numerically evaluated trajectory.

4 Poincaré sections

Poincaré sections are a key tool for analyzing chaotic systems. A *Poincaré section* is defined as a hyper-surface in the phase space of a system such that not trajectories are tangential to the surface (i.e. no trajectories run along the surface). A *Poincaré map* with respect to a given Poincaré section by sampling a trajectory of the system every time it passes through the Poincaré section. A Poincaré map for a continuous dynamical system converts it into a discrete time map of one less dimension. As we'll see, reduction of dimension helps us visualize the flow better. The Poincar'e map can also be used to perform stability analysis for periodic orbits.

4.1 Poincaré map for the Duffing oscillator

Because the Duffing oscillator is periodically forced, computing the Poincaré map is easy - we simply sample a trajectory once every period of the driving force. Firstly, recall that our state space is,

$$\mathcal{M} = \{ \begin{bmatrix} q \\ p \\ z \end{bmatrix} : q, p \in \mathbb{R}, z \in [0, 2\pi) \}.$$

Let the f^t be the time evolution function such that $f^t(x(0)) = x(t)$ for any $x(0) \in \mathcal{M}$. The Poincaré section for the Duffing oscillator is

$$\mathcal{S} = \{ \begin{bmatrix} q \\ p \\ z \end{bmatrix} : z = 0 \}.$$

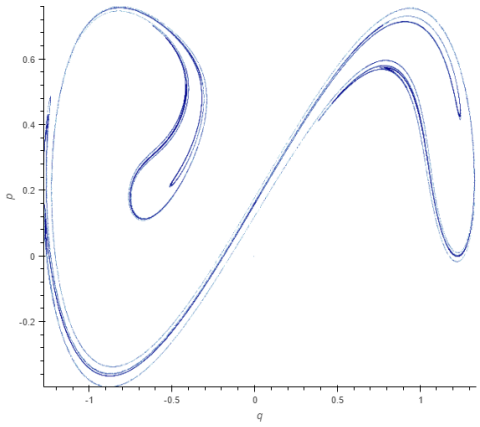

Figure 6: Strange attractor for the Duffing oscillator at parameters $(b, A, \Omega) = (0.15, 0.35, 1)$.

Any point $\mathbf{r} \in \mathcal{S}$ will be of the form $\mathbf{r} = (q, p, 0)$. A tangent vector $\mathbf{t} \in \mathcal{M}$ to $\mathcal{S}$ at $\mathbf{r}$ will be of the form $\mathbf{t} = (x, y, 0)$ for any $x, y \in \mathbb{R}$.The displacement that $\mathbf{r}$ experiences in an infinitesimal time δt is,

$$\delta\mathbf{r} = f^{\delta t}(\mathbf{r}) - \mathbf{r} = \begin{bmatrix} q(\delta t) \\ p(\delta t) \\ \delta t \end{bmatrix}.$$

$\delta\mathbf{r} \neq (x, y, 0)$ for any $x, y \in \mathbb{R}$, so is not a tangent to $\mathcal{S}$. This shows that there are no trajectories tangent to $\mathcal{S}$, hence, $\mathcal{S}$ satisfies the definition we gave for a hyper-surface to be a Poincaré section.

The Poincaré map $P : \mathcal{S} \to \mathcal{S}$ for the Duffing oscillator is then defined

$$P(\mathbf{r}) = f^{\frac{2\pi}{\Omega}}(\mathbf{r}).$$

In practice, this map must be evaluated numerically using a computer. In the previous section, we claimed that the Duffing oscillator was chaotic for parameters $(b, A, \Omega) = (0.15, 0.35, 1)$.

If the continuous system tends to a fixed point the the Poincaré map must also tend to a fixed point. A periodic orbit for the Duffing oscillator (for non-zero driving force) must have a period of a positive integer multiple of the driving force period. This is because the Poincaré map fully defined the system and if the period of an orbit is not an integer multiple of the driving force then it will not be a periodic orbit for the Po incé map. Therefore, a periodic orbit corresponds to either a fixed point, or a period-n cycle in the phase space. For the parameters $(b, A, \Omega) = (0.15, 0.1, 1)$, the system in general either tends to a periodic orbit around $\mathbf{u}_+$ or a periodic orbit around $\mathbf{u}_-$. These both have a period of 2π, so correspond to fixed points at $\mathbf{u}_+$ and $\mathbf{u}_-$ in the Poincaré map.

Figure 6 shows a plot of a trajectory of 100,000 points of the Poincaré map evolved from the initial condition $\mathbf{u}_0$. The reduction of dimensionality induced by the Poincaré map allows us to see the flow of the system more clearly, although the trajectory seems completely random it tends towards the geometric object in figure 6, called a strange attractor. The strange attractor is in fact a fractal, meaning that it exhibits self similarity and has a non-integer fractal dimension. As we zoom into the strange attractor we see more and more structure. In fact in a fractal there is structure no matter how small the scale is. This is the first piece of evidence that the Duffing oscillator is chaotic at these parameters. In section ??, we estimate the fractal dimension of the strange attractor and demonstrate that it is indeed a fractal set.

5 Lyapunov exponent

5.1 Definition

A system that is bounded and displays sensitive dependence to initial conditions can be considered chaotic. A system displays sensitive dependence to initial conditions if two trajectories initially separated by an infinitesimal distance separate $|\delta\mathbf{r}(0)|$ diverge exponentially,

$$|\delta\mathbf{r}(t)| \approx |\delta\mathbf{r}(0)| \exp(\lambda t), \tag{9}$$

with $\lambda > 0$. λ is the mean rate of separation and is known as the *leading Lyapunov exponent*, which we will call simply the Lyapunov exponent. The Lyapunov exponent can also written in terms of the initial separation at time t as the initial separation tends to zero and the time tends to infinity,

$$\lambda = \lim_{t\to\infty} \lim_{\delta r\to 0} \frac{1}{t} \ln(\frac{|\delta\mathbf{r}(t)|}{|\delta\mathbf{r}(0)|}). \tag{10}$$

The Duffing oscillator is bounded for all parameters. This is because the double well potential tends to infinity as $q \to \pm\infty$. Therefore to show that the system is chaotic at parameters $(b, A, \Omega) = (0.15, 0.35, 1)$, we need to show that the Lyapunov exponent is positive,

5.2 Numerical estimation of the Lyapunov exponent

To evaluate the Lyapunov exponent (10), we first choose two initial conditions $\mathbf{r}_1(0)$ and $\mathbf{r}_2(0)$ separated by some very small distance r_{min} at random angle in phase space . We then evolve the two trajectories until either:

1. The separation of the two trajectories reach some maximum distance r_{max}, or,
2. The maximum time t_{max} is reached .

When one of these two conditions is met, we record the time t_1 and the maximum distance between the trajectories r_1.The we the first approximation for the Lyapunov exponent will be,

$$\lambda_1 = \frac{1}{t_1} \ln(\frac{r_1}{r_{min}}).$$

To obtain a better approximation we reset the second trajectory so that it is again a distance r_{min} from $\mathbf{r}_1(t_1)$ at a random angle. We evolve the trajectories again until either condition 1 or condition 2 is met again recording the time taken (from the time it was last reset) and the maximum separation. We denote the time taken for one of the conditions to be met after the $(i-1)$th reset by t_i and the maximum separation when its met by r_i. Then the nth approximation to the Lyapunov approximation is,

$$\lambda_n = \frac{1}{t} \sum_{i=1}^{n} \ln(\frac{r_i}{r_{min}}).$$

The larger n is, the better the approximation.

The method above is a variation of the most basic method described in chapter 6 of [2]. The key difference is that we have two conditions. The r_{max} condition ensures that the separation for chaotic systems with an extremely fast rate of separation does not get too large. The t_{max} condition ensures that when measuring the Lyapunov exponent of non-chaotic systems where the separation decrease with time, the trajectories do eventually reset.

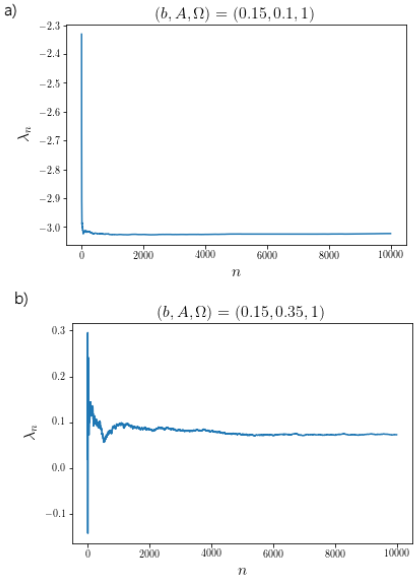

Figure 7: a) Running approximation for the leading Lyapunov exponent at non-chaotic parameters $(b, A, \Omega) = (0.15, 0.1, 1)$. b) Running approximation for the leading Lyapunov exponent at chaotic parameters $(b, A, \Omega) = (0.15, 0.35, 1)$.

In general, we want r_{max} to be as large as possible while still small enough so that the separation can be approximated by the linear term in a Taylor series. This is because equation (9) is valid in this linear region and once the separation becomes near the size of the strange attractor, it must reduce in order for the system to be bounded. (**Remark** : To determine r_{max} we plotted a slice of the distance-squared moved function $\Delta(\mathbf{r}) := |P(\mathbf{r}) - \mathbf{r}|$ around an unstable periodic orbit for the chaotic parameters. r_{max} was chosen so that this slice of Δ was still appropriately approximated by a quadratic function at a distance $r_{max}$from the unstable periodic orbit.) We chose a value of $r_{max} = 0.01$ for the maximum separation. The minimum separation was chosen to be as small as possible while still reaching the maximum separation in a reasonable time. We chose $r_{min} = 0.00001$. With this value for the minimum separation, the maximum separation was reached in approximately 10 periods of the driving force for the chaotic parameters. The maximum time was chosen to be approximately the time that the trajectories took to reach the maximum separation for the chaotic parameters.

5.3 Results

We implement the code in python. The code is shown in Appendix ??. The code comes in the form of a function which takes 3 arguments. The first argument is a 2-D array of the initial condition $[q, p]$. The

second is a 3-D array of the parameters $[b, A, \Omega]$. The third is a positive integer N for the maximum number of approximations we make. The function returns an array with a running approximation of Lyapunov exponents, $[\lambda_1, ..., \lambda_N]$. λ_N is taken as the final approximation of the Lyapunov exponent.

We applied this function for the parameters $(b, A, \Omega) = (0.15, 0.1, 1)$, for which the trajectories converged to a limit cycle. The maximum number of approximations was 10,000. The running approximation for the Lyapunov exponent is shown in figure 7a). It clearly seems to converge. The final approximation for the Lyapunov exponent was $\lambda = -3.02$. Which is negative as expected, indicating that the system is not chaotic for these parameters.

We also applied the function for the parameters $(b, A, \Omega) = (0.15, 0.35, 1)$. The maxim number of approximations was again 10,000. The running approximation for the Lyapunov exponent, shown in figure 7b), again seems to converge nicely. The final approximation for the Lyapunov exponent was λ =0.073, which is positive,as expected.

6 Fractal dimensionality of the strange attractor

The attractor for the Duffing oscillator are parametes $(b, A, \Omega) = (0.15, 0.35, 1)$ (figure 6) exhibits fractal properties such a self similarity. A fractal attractor (i.e. a strange attractor) is a classic indication that the dynamics are chaotic. To test whether the attractor is indeed a fractal, we need to estimate the fractal dimension of the attractor. We define the fractal dimension to be the *box counting dimension.*

6.1 Definition

Let $\mathcal{F} \subset \mathbb{R}^2$ be a set in 2-dimensional Euclidean space. Partition the $\mathbb{R}^2$ into almost disjoint squares of size ϵ, so that the squares form a grid in $\mathbb{R}^2$. Let $N(\epsilon)$ be the number of squares of size ϵ that contain at least one point in $\mathcal{F}$. Then the box counting dimension of $\mathcal{F}$ is defined as

$$D(\mathcal{F}) = \lim_{\epsilon \to 0} \frac{\ln(N(\epsilon))}{\ln(\frac{1}{\epsilon})}. \tag{11}$$

Consider a closed unit interval $I = [0, 1]$ in $\mathbb{R}^2$. Then when $\epsilon_n = \frac{1}{n}$,the number of boxes containing a point in $\mathbb{R}^2$ is

$$N(\epsilon_n) = n.$$

Then by (11), the box counting dimension of I is

$$\begin{aligned} D(I) &= \lim_{n \to \infty} \frac{\ln(N(\epsilon_n))}{\ln(1/\epsilon_n)} \\ &= \lim_{n \to \infty} \frac{\ln(n)}{\ln(n)} \\ &= 1. \end{aligned}$$

In fact any curve in $\mathbb{R}^2$ has a box counting dimension of 1 [4]. A fractal is defined as a geometric object which has a non-integer box-counting dimension.

6.2 Results

We implemented an algorithm that calculates the box-counting dimension in python in the form of a fun unction boxcounting_dim which takes 2 arguments. The first is the data set which we wish to calculate the box counting dimension of. The second is the number of boxes from one side of the grid to the other. The main computationally expensive task was calculating $N(\epsilon)$. This was achieved using a function from datashader, a python package for plotting large data sets that we also used to plot bifurcation diagrams (see next section). Essentially package includes a function which counts the amount of points in each box of the grid, and returns a 2-d array with this data. Our algorithm then simply counts the number of non-zero elements in this array to obtain $N(\epsilon)$. The advantage of using the datashader package was that the package was optimized to run quickly even on huge data sets, hence was far faster than any algorithm for calculating $N(\epsilon)$ that we could develop in a reasonable time frame.

To test that our algorithm worked properly, we generated two test data sets for which we knew the dimension of. The first data set was 100,000 points forming a unit interval. The dimension is analytically known to be 1. The other set was the Hénon attractor[3] . The Hénon map is an analytically defined chaotic map which has a strange attractor for variance parameters. The literature value of the box counting dimension for the strange attractor is 1.3 for the specific parameters we used[6]. The Hénon attractor data set also contained 100,000 points. The advantage of using the Hénon attractor as a testing ground is that it is a similar object (an attractor for a chaotic map) to the attractor in figure 6. Our algorithm returned a value of $D = 1.00$ to two decimal places for the box counting dimension of the unit interval. We used a grid with 5000 boxes per side. This is promising because it indicates that our algorithm does not return non-integer values for the fractal dimension for non-fractal sets. Our algorithm returned a box counting dimension of $D = 1.28$ to 2 decimal places for the Hénon map, again using 5000 boxes per side of the grid. This is within 0.02 of the literature value. This is very acceptable because the literature value is only approximate and we we are are mainly look to demonstrate the existence of fractal dimensionality; the specific value is not so important.

To be consistent with the two tests the data set for the Duffing attractor consisted of 100,000 points, just like the test data sets. We also used 5000 boxed per side as before. Our algorithm returned an estimation of $D_{duff} = 1.15$ for the box counting dimension of the Duffing attractor in question. D_{duff} is a non-integer value, indicating that the attractor is a fractal. This value is in the same ball park as the Hénon attractor, which supports the value because the Hé non attractor looks qualitatively similar to the Duffing attractor. D_{duff} is not too close to 2 also. This supports the estimation because a fractal close to a dimension of 2, embedded in 2 dimensions, would be space-filling which the Duffing attractor clearly is not.

7 Bifurcation diagram

Bifurcation diagrams are a tool to investigate how the qualitative behavior of a system changes as a parameter is changed. In section 4, we found that the behavior of the system changed as we varied A while keeping the other two parameters fixed. For most values of A a small change in A only produced a small change in the qualitative behavior of the system. For example, the the non-chaotic region around $A = 0.1$, a small increase A led to a small increase in the width of the limit cycles in phase space. In the chaotic region around $A = 0.35$, a small increase or decrease in the value of A produced a small deformation of strange attractor. However, for some values of A, a small change caused a drastic change in the qualitative behavior of the system. For example, at $A = 0$, a small increase in A meant that the stable fixed point were destroyed and replaced by limit cycles. Also the onset set of chaos was very sudden and seemed to occur just as the trajectories had enough energy to jump between wells. The points where an infinitesimal change in a parameter causes a

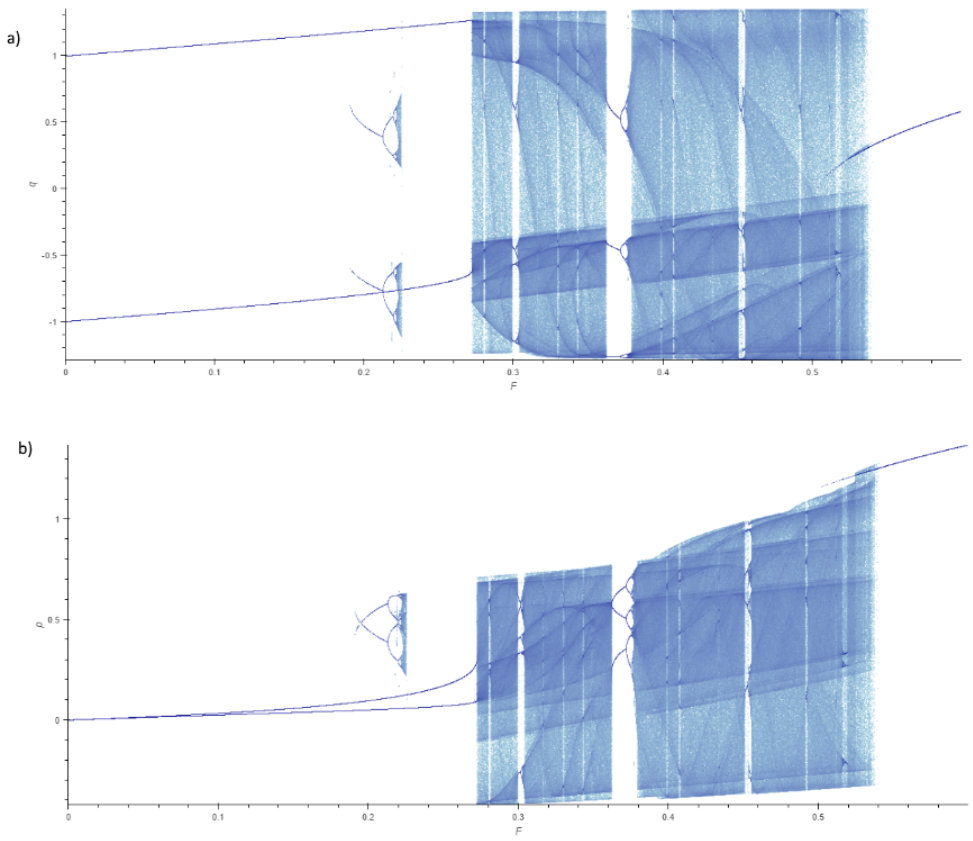

Figure 8: Bifurcation diagrams for the Duffing osllator with the parameters $b = 0.15$ and $\Omega = 1$ fixed.

qualitative change in the behavior of the system are called *bifurcation points.*

A bifurcation diagram, is a plot with a parameter on the x-axis and one dimensional projection of the attractor at that value of the parameter plotted along the y-axis.

In our case we varied F from $F_{min} = 0$ to $F_{max} = 0.6$, while keeping the damping fixed at $b = 0.15$ and keeping the the frequency fixed at $\Omega = 1$. We chose 6000 evenly spaced F values between 0 and 0.6. The set of values for F we sampled was,

$$S_F = \{0.001n : 0 \leqslant n \leqslant 6000\}.$$

Then for each $F_i \in S_F$, we generated a random set of 9 initial conditions such that magnitude of the q value was less than 1.5 and such that the p values are less than 1. These values were based on the size of the strange attractor in figure 6. We then evolved each of these random initial conditions 100 returns. This was to ensure that the system settled down to the attractor. Then next 100 returns were added to the set $S_{bif}(F_i)$. The set $Q_{bif}(F_i)$ contained only the q values of $S_{bif}(F_i)$ and The set $P_{bif}(F_i)$ contained only the p

values of $S_{bif}(F_i)$. The final bifurcation diagram for q was the set

$$Q_{bif} = \{\bigcup_i Q_{bif}(F_i) : F_i \in S_F\}.$$

The final bifurcation diagram for p was the set

$$P_{bif} = \{\bigcup_i P_{bif}(F_i) : F_i \in S_F\}.$$

The above algorithm was implemented in python. The final data set contained over 5 million points for each bifurcation diagram. The bifurcation diagram was plotted using the python package datashader, which shades each pixel depending on how many points are in the corresponding region. The final bifurcation diagram is shown in figure **??**.

7.1 Analysis of the Bifurcation diagram

The specific Bifurcation diagram that we will refer to is the one for q, shown in figure **??** a). We begin our analysis of the bifurcation diagram by noting that at $A = 0$. The slice of the attractor (what we formally defined as $Q_{bif}(0)$), is two points at $q = -1$ and $q = 1$. This corresponds to the fixed points at $\mathbf{u}_+$ and $\mathbf{u}_-$ in the absence of driving force (recall that fixed points in the continuous system are also fixed points in the Poincaré map). Now, from $A = 0$ to around $A = 0.28$ we see two dark lines. These are stable period-1 (in terms of 2π) limit cycles that grow in size as we increase A. We then see a very drastic bifurcation into the chaotic regime. Using an interactive, which re-renders the image with updated axis as we zoom in, we obtained a value of $A_{chaos} = 0.273 \pm 0.001$ for this Bifurcation point. Evidence of strange attractor are clearly visible inside the chaotic region and we can see the strange attractor deforming as A changes. At certain points in the chaotic region, the faction diagram briefly becomes a prime number of lines (e.g. 3 and 5 are clearly visible), corresponding to a stable limit cycle appearing. This is very characteristic of chaotic systems and this phenomenon of a window of calm among chaos can also be seen in bifurcation diagrams for the logistics map [4]. The limit cycle in these windows undergo a cascade of period doubling back into chaos.

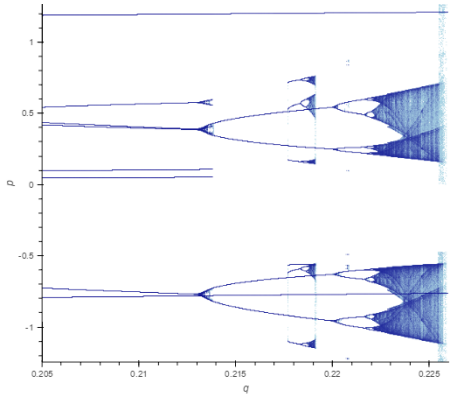

Figure 9: A zoom of the Bifurcation digram for the region $A = 0.205$ to $A = 0.226$.

Now we investigate the region around $A = 0.2$ to $A = 0.226$. At around $A = 0.2$, new limit cycles appear even in the pretense of the two main stable limit cycles. We then observe the lines split. This is known as period-doubling. In this case, it corresponds to a limit cycle splitting up into two new limit cycles. We observe that period doubling occurs many more times in the system with the distance between period doubling events getting shorter each time. Eventually there are infinitely many unstable periodic orbits and the system becomes chaotic. This again is observed in many chaotic systems. Let d_i be the distance between the ith and $(i+1)$th period doubling event. In the logistics map the distances converge to a constant called Feigenbaum's constant,

$$\lim_{i\to\infty} \frac{d_i}{d_{i+1}} \approx 4.67.$$

	Locations		Duffing Estimates
a_1	0.213	$\frac{d_2}{d_1}$	4.44±0.18
a_2	0.2201	$\frac{d_3}{d_2}$	4.32±0.34
a_3	0.2217	$\frac{d_4}{d_3}$	4.63±0.68
a_4	0.22207		
a_5	0.22215		

Table 1: Estimation of Feigenbaum's constant

Eigenvalue hypothesized the universality of this constant, meaning that it appears in a large variety of systems.(REFERENCE) Here we test we d_i/d_{i+1} approaches Feigenbaum's constant for the period doubling cascade between $A = 0.2$ and $A = 0.226$. We produced a high resolution zoom of this region shown in figure 9. The lines seem to broaden where the period doubling occurs. This cud be because the trajectories airless inclined to settle down to a limit cycle when there are two that are very close together.
Table 1 shows the results a_1 to $a_5$are the measure A values for the period doubling and in the next column we have the first 3 estimations for Feigenbaum's constant. Even though the uncertainties are large the values seem to match quite well with the logistics map estimates [1]. The results definitely not conclusive, however, there is some evidence that the period doubling cascade does obey Feigenbaums constant. To calculate the constant better we would need a higher resolution bifurcation diagram, where we let the trajectories settle down for longer before sampling, to reduce broadening.

8 Symmetry

Finally, we study the symmetries of the Duffing oscillator. This analysis is based on [2] chapter 9. The dimension of the Duffing oscillator is three, in the sense that there are three equations in the equation of motion when put into autonomous form. Now suppose for contradiction that there does exist a continuous symmetry for Duffing oscillator. Then, by Noether's theorem there will be a conserved quantity associated to that symmetry. This conserved quantity will reduce the dimension of the system by one, reducing the state-space to two dimensions. Then, by Poincaré-Bendixson theorem a continuous dynamical system with a two dimensional state space cannot exhibit chaos . However, we know that the Duffing oscillator does exhibit chaos in certain parameter regimes, therefore, there does not exist any continuous symmetries for the Duffing oscillator.

However, there does exist at least one discrete symmetry for the Duffing oscillator as we will now demonstrate, following the theory presented in [discrete]. Consider the Duffing oscillator with the driving force A set to zero. Then, if we start the system at some point $q_0 > 0$ with zero velocity the system will eventually reach the bottom of the right well $q_1 > 0$. Let's say it does this in a time τ_0. The double well is symmetric when reflected along $q = 0$, we can say it is invariant under the transformation $q \to -q$. This symmetry allows us to immediately say something about another a trajectory - if we start at $-q_0$ then the state will reach the bottom of the left well in time τ_0. In more generality, if $(q(t), p(t))$ with initial conditions (q_0, p_0), is the first trajectory then if we start from $(-q_0, -p_0)$, the trajectory will be $(-q(t), -p(t))$. The Duffing oscillator with A set to zero is invariant under the transformation $(q, p) \to (-q, -p)$, the reversal of p ensures the damping forces remains equivalent for the transformed and original trajectories. When we introduce the driving force, this symmetry is broken. To see this, suppose for the initial condition $q_0 > 0$ the driving force is initially towards the nearest well. When we start from the initial condition $-q_0$, the driving force will be away the the

nearest well, clearly yielding a non-equivalent trajectory. To retain symmetry, we must also transform the time forwards by π/ω. Then, the driving force is transformed as $A\cos(\Omega t) \to A\cos(\Omega t + \pi) = -A\cos(\Omega t)$. Now, let ϕ be the transformation describes previously,

$$\phi \begin{bmatrix} q \\ p \\ z \end{bmatrix} = \begin{bmatrix} -q \\ -p \\ z + \pi \end{bmatrix}.$$

Then,

$$\begin{aligned} &\frac{d}{dt}(\phi \begin{bmatrix} p \\ x \\ z \end{bmatrix}) = \mathbf{f}(\phi \begin{bmatrix} p \\ x \\ z \end{bmatrix}). \\ \Leftrightarrow &\frac{d}{dt}(\begin{bmatrix} -q \\ -p \\ z \end{bmatrix}) = \begin{bmatrix} -p \\ -(-2bp + q - q^3 + A\cos(z)) \\ \omega \end{bmatrix} \\ \Leftrightarrow &\frac{d}{dt}(\begin{bmatrix} q \\ p \\ z \end{bmatrix}) = \begin{bmatrix} p \\ -2bp + q - q^3 + A\cos(z) \\ \omega \end{bmatrix} \\ \Leftrightarrow &\frac{d}{dt}(\begin{bmatrix} p \\ x \\ z \end{bmatrix}) = \mathbf{f}(\begin{bmatrix} p \\ x \\ z \end{bmatrix}). \end{aligned}$$

So, if $(q(t), p(t))$ is a solution for the Duffing oscillator then we get another solution $(-q(t+\frac{\pi}{\Omega}), -p(t+\frac{\pi}{\Omega}))$ for free. In particular, if we have identified a periodic orbit $(q(t), p(t))$ (so that $(q(t), p(t)) = (q(t+\tau), p(t+\tau))$ for some τ) then $(-q(t+\frac{\pi}{\Omega}), -p(t+\frac{\pi}{\Omega}))$ is also a periodic orbit of the same period. Notice that $\phi \circ \phi = \iota$ where ι is the identity transformation, so $G = \{\iota, \phi\}$ forms a group. The technical terms for the symmetry described is G equivariance.

Numerical test confirm that this symmetry exist. For a Poincaré section

$$\mathcal{S}_\pi = \{ \begin{bmatrix} q \\ p \\ z \end{bmatrix} : z = \pi \}$$

The corresponding strange attractor (for example for the parameters $(b, A, \Omega) = (0.15, 0.35, 1)$) is exactly the strange attractor generated by the Poincaré section $\mathcal{S}$ (from section 5) reflected along the line $\{(q, p) : q = p\}$ (reflection along this line takes $q \to -q$ and $p \to -p$).

9 Conclusions

The Duffing oscillator offers a rich variety of dynamical behavior and this report hardly scratches the surface. The main results of this report are summarized as followed:

- The Lyapunov exponent was measured to be postie in the chaotic regime and negative in the non-chaotic regime.
- The box counting dimension dimension of the attractor in a chaotic regime was measured to be a non-integer.

- Period doubling cascades in the bifurcation diagram seem to obey the universality of Feigenbaum's constant.
- There are no continuous symmetries for the Duffing oscillator, however there is at least one discrete symmetry.

For further investigation we suggest investigating the region for which we studied the period doubling cascade, is this region chaotic for certain initial conditions? There is evidence that there is an infinite number of unstable periodic orbits, due to the period doubling cascade in the windows of calm. How can we find and classify the stability of these unstable periodic orbits? Can we use them to further understand or make calculations about the system?

References

[1] Keith Briggs. A precise calculation of the feigenbaum constants. *Mathematics of Computation*, 1991.

[2] P. Cvitanović, R. Artuso, R. Mainieri, G. Tanner, and G. Vattay. *Chaos: Classical and Quantum*. 2016.

[3] M. HÃ©non. A two-dimensional mapping with a strange attractor. *Communications in Mathematical Physics*, 1976.

[4] Edward Ott. *Chaos in dynamical systems*. 1993.

[5] Steven Strogatz. *Nonlinear dynamics and Chaos*. 1994.

[6] James Theiller. Estimating the fractal dimension of chaotic time series. *The Lincoln Laboratory Journal*, 3(1), 1990.